



On the rotation of a circular porous particle in 2D simple shear flow with fluid inertia

Chengong Li¹, Mao Ye^{1,†} and Zhongmin Liu¹

¹Dalian National Laboratory for Clean Energy, National Engineering Laboratory for MTO, iChEM (Collaborative Innovation Center of Chemistry for Energy Materials), Dalian Institute of Chemical Physics, Dalian, 116023, China

(Received 10 July 2016; revised 9 October 2016; accepted 11 October 2016; first published online 2 November 2016)

We investigate numerically the rotational behaviour of a circular porous particle suspended in a two-dimensional (2D) simple shear flow with fluid inertia at particle shear Reynolds number up to 108. We use the volume-averaged macroscopic momentum equation to formulate the flow field inside and outside the moving porous particle, which is solved by a modified single relaxation time lattice Boltzmann method. The effects of fluid inertia, confinement of the bounding walls, and permeability of the particle are studied. Our two-dimensional simulation results confirm that the permeability has little effect on the rotation of a porous particle in unbounded shear flow without fluid inertia (Masoud, Stone & Shelley, *J. Fluid Mech.*, vol. 733, 2013, R6), but also suggest that the role of permeability cannot be neglected when the confinement effect is significant, or the fluid inertia is not negligible. The fluid inertia and the confined walls have similar effects on the rotation of a porous particle as that on a solid impermeable particle. The angular velocity decays with an increase in fluid inertia, and the confinement effect suppresses the angular velocity to a shear rate ratio below 0.5. A simple scaling argument based on the balance of torque exerted by fluid flows adjacent to the two bounding walls and that due to the flow recirculation can explain our results.

Key words: porous media, suspensions, particle/fluid flow

1. Introduction

Rotation of particles at finite particle shear Reynolds number (Re_p), which is essential to understanding the hydrodynamics of particle–fluid systems in many industrial and natural processes, has been the subject of a variety of theoretical (Lin, Peery & Schowalter 1970; Robertson & Acrivos 1970), experimental (Poe & Acrivos 1975; Zettner & Yoda 2001; Bluemink *et al.* 2008), and numerical studies (Kossack & Acrivos 1974; Ding & Aidun 2000; Ku & Lin 2009; Mao & Alexeev

[†] Email address for correspondence: maoye@dicp.ac.cn

2014). Moreover, several advancements have been made recently on detecting and tracking particle rotation (Zimmermann *et al.* 2011; Klein *et al.* 2013; Byron *et al.* 2015; Wu *et al.* 2015; Mathai *et al.* 2016). These studies exclusively focused on impermeable particles. In practice, however, porous and permeable particles are frequently encountered. Examples include coal particles in power stations, suspended sediment in coastal waters, and catalyst clusters in fluidized bed reactors. The permeability of the particle can affect the flow pattern as well as particle–fluid interactions to various extents (Chen & Cai 1999; Bhattacharyya, Dhinakaran & Khalili 2006; Shahsavari, Wardle & McKinley 2014). Nonetheless, there have been no investigations about the rotation of porous particles in fluid flow, apart from a very recent theoretical analysis by Masoud, Stone & Shelley (2013) on the rotation of porous ellipsoids in an unbounded simple shear flow. Their analysis was based on the coupled Brinkman–Stokes model (Debye & Bueche 1948). They found that the permeability has little effect on the rotation of porous particles in the absence of fluid inertia, and Jeffery’s prediction (Jeffery 1922) remains an excellent approximation for the angular velocity of porous ellipsoids in simple shear flow without fluid inertia. Previous studies showed that the effect of fluid inertia, which increases with Re_p , leads to a reduction of angular velocity for a solid impermeable particle in shear flow (Lin *et al.* 1970; Poe & Acrivos 1975; Ding & Aidun 2000; Zettner & Yoda 2001). Therefore, the natural question is how the permeability affects the rotation of porous particles in shear flow with fluid inertia.

In order to describe fluid flow through a porous medium, models based on either Darcy’s law or the Brinkman equation have been widely employed (Brinkman 1949; Neale & Epstein 1973; Michalopoulou, Burganos & Payatakes 1993; Ollila, Ala-Nissila & Denniston 2012; Dalwadi *et al.* 2016). Compared to Darcy’s law, the Brinkman equation includes a viscous term in the momentum equation to account for the boundary layer occurring in porous medium flow, and thus the continuity of fluid velocity and shear stress is fulfilled at the interface between the porous region and the free flow. Many researchers have used the Brinkman equation to study the flow past moving porous media (Debye & Bueche 1948; Roy & Damiano 2008; Masoud *et al.* 2013). However, these studies were limited to fluid flows with low enough Reynolds number, such as creeping flow, because no nonlinear inertial term has been included in the Brinkman equation. The inertial effect on the fluid flow of a moving porous medium is not minute in practical applications (Wood 2007). Recently, Wang *et al.* (2015) presented a volume-averaged macroscopic momentum equation in terms of the intrinsic phase-average velocity for fluid flow passing the porous medium, in which they included the inertial terms; thus, this equation is suitable for fluid flow with finite Re_p .

In this work, we study the rotation of a circular porous particle in a simple shear flow with Re_p up to 108. The general volume-averaged macroscopic governing equations of Wang *et al.* (2015) are used to formulate the fluid flow around and inside the porous particle. A lattice Boltzmann model is adopted to numerically solve the general macroscopic equations. The effects of fluid inertia, confinement by the boundary walls, and permeability of the particle are investigated. Our results reveal that the fluid inertia and confinement of the bounding walls affect the rotation of a porous particle in shear flow in a similar way to that of a solid impermeable particle. Although the permeability has a negligible effect on the angular velocity of a porous particle in unbounded shear flow at very low Re_p , as found by Masoud *et al.* (2013), our results suggest that the permeability is of paramount importance in porous particle rotation in shear flow with either a significant confinement effect or a finite particle shear Reynolds number.

2. Method

2.1. Governing equations

Here, we consider one single, circular, neutrally buoyant, porous particle rotating in a simple shear flow. The particle is placed in the centre of a rectangular channel of length L and width H . The fluid flow is driven by two bounding walls (located in the width direction) moving at the same speed U , but in opposite directions. The particle shear Reynolds number is defined as $Re_p = GD^2/\nu$, where D is the particle diameter, $G = 2U/H$ is the shear rate, and ν is the fluid kinematic viscosity. We adopt the volume-averaged macroscopic equations in terms of the intrinsic phase-average velocity to formulate the porous particle–fluid system (Wang *et al.* 2015). The macroscopic equations consist in averaging the microscopic equations over a representative element volume (REV), where the REV scale is much larger than the characteristic size of pore structures, such that it includes sufficient pores for the averaging. On the other hand, however, it should be much smaller than the particle such that the volume-averaged macroscopic equation can be applied in the porous domain of the particle. Therefore, the fluid flow is governed by the following macroscopic equations

$$\nabla \cdot \langle \mathbf{u}_f \rangle^f = 0 \quad \text{and} \quad \frac{\partial \langle \mathbf{u}_f \rangle^f}{\partial t} + \langle \mathbf{u}_f \rangle^f \cdot \nabla \langle \mathbf{u}_f \rangle^f = -\frac{1}{\rho_f} \nabla \langle p_f \rangle^f + \nu \nabla^2 \langle \mathbf{u}_f \rangle^f + \mathbf{F}_m, \quad (2.1)$$

where ρ_f is the fluid density, and $\langle \mathbf{u}_f \rangle^f$ and $\langle p_f \rangle^f$ are the intrinsic phase-average velocity and pressure of fluid phase, respectively. The total body force \mathbf{F}_m is calculated via

$$\mathbf{F}_m = -\frac{\varepsilon \nu}{K} (\langle \mathbf{u}_f \rangle^f - \langle \mathbf{u}_s \rangle^s) - \frac{\varepsilon^2 F_\varepsilon}{\sqrt{K}} (\langle \mathbf{u}_f \rangle^f - \langle \mathbf{u}_s \rangle^s) |\langle \mathbf{u}_f \rangle^f - \langle \mathbf{u}_s \rangle^s| + \mathbf{G}, \quad (2.2)$$

where $\langle \mathbf{u}_s \rangle^s$ is the intrinsic phase-average velocity of particle, and ε the porosity of particle. In the limit of $\varepsilon = 0$, the porous particle reduces to a solid impermeable particle, whereas as ε approaches 1, the porous regime would be filled by fluid and \mathbf{F}_m vanishes in (2.1). K is the permeability of particle, which qualifies the ability of the porous medium to transmit fluids, which is denoted by the Darcy number, $Da = K/D^2$, in this work. The geometric function F_ε follows Ergun's correlation (Ergun 1952), $F_\varepsilon = 1.75/\sqrt{150\varepsilon^3}$. Note that the porous structure inside the porous particle is described by the permeability and the porosity. In this work, for simplicity, we associate the permeability K with the porosity ε via $K = \varepsilon^3 d_p^2/[150(1 - \varepsilon)^2]$, where d_p stands for the characteristic diameter of filling grains within the porous particle, which is taken as 100 μm here, following Bhattacharyya *et al.* (2006). The total body force \mathbf{F}_m includes the resistance arising due to the porous medium, and the external body force \mathbf{G} . On the right-hand side of (2.2), the first and the second terms represent the linear and nonlinear drag force, respectively. Under creeping flow conditions, i.e., steady flow with a sufficiently low flow velocity, the nonlinear resistance can be neglected because of its quadratic nature. Thus, the inertial term in (2.1) can be omitted. The macroscopic equations (2.1) reduce to the coupled Brinkman–Stokes model (Debye & Bueche 1948) in the absence of an external body force. The net force \mathbf{F}_p and torque \mathbf{T}_p on the particle are calculated using Newton's equations:

$$\mathbf{F}_p = M_p \frac{d\mathbf{V}_p}{dt} = - \int_S \mathbf{n} \cdot \boldsymbol{\sigma} \, ds \quad \text{and} \quad \mathbf{T}_p = I_p \frac{d\boldsymbol{\omega}_p}{dt} = - \int_S (\mathbf{r}_b - \mathbf{R}) \times (\mathbf{n} \cdot \boldsymbol{\sigma}) \, ds, \quad (2.3a,b)$$

where M_p is the particle mass, I_p the moment of inertia of particle, and S the boundary of the particle. Note that \mathbf{r}_b represents the position vector of boundary node, \mathbf{R} the position vector of particle centre, $\boldsymbol{\sigma}$ the stress tensor, \mathbf{n} the unit outward normal vector, $\mathbf{F}_p^{drag} = \int_S \mathbf{n} \cdot \boldsymbol{\sigma} ds$ the hydrodynamic drag force experienced by particle, $\boldsymbol{\omega}_p$ the angular velocity of particle, and \mathbf{V}_p the simple expression of $\langle \mathbf{u}_s \rangle^s$. The velocity of particle \mathbf{u}_s is defined as $\mathbf{u}_s = \mathbf{U}_p + \boldsymbol{\omega}_p \times (\mathbf{r} - \mathbf{R})$, with \mathbf{U}_p and \mathbf{r} being the translation velocity and position vector of the particle, respectively.

2.2. Numerical approach

The lattice Boltzmann method has been successfully applied to simulate complex fluid flows because of its easy implementation of boundary conditions, short codes, and natural parallelism compared to conventional computational methods based on the Navier–Stokes equations (Ladd 1994; Zou & He 1997; Chen & Doolen 1998; Ding & Aidun 2000; Ollila *et al.* 2012; Mao & Alexeev 2014; Wang *et al.* 2015). In this work we use a modified single relaxation time lattice Boltzmann equation (SRT-LBE) model to solve equations (2.1). The corresponding lattice Boltzmann evolution equations are given as

$$f_\alpha(\mathbf{x} + \mathbf{e}_\alpha \delta t, t + \delta t) - f_\alpha(\mathbf{x}, t) = -\frac{1}{\tau} [f_\alpha(\mathbf{x}, t) - f_\alpha^{eq}(\mathbf{x}, t)] + \delta t F_\alpha, \quad (2.4)$$

where τ is the relaxation time, $f_\alpha(\mathbf{x}, t)$ the particle distribution function (PDF), $f_\alpha^{eq}(\mathbf{x}, t)$ the equilibrium PDF and F_α the force term. In our simulations, the two-dimensional nine velocities (D2Q9) model is used. The lattice speed c is given by $c = \delta x / \delta t$, where δx is the lattice size, and δt the time step. The equilibrium PDF and the force term are defined as

$$f_\alpha^{eq}(\mathbf{x}, t) = \rho_f \omega_\alpha \left[1 + \frac{\mathbf{e}_\alpha \cdot \mathbf{u}}{c_s^2} + \frac{(\mathbf{e}_\alpha \cdot \mathbf{u})^2}{2c_s^4} - \frac{u^2}{2c_s^2} \right], \quad (2.5)$$

$$F_\alpha = \rho_f \omega_\alpha \left(1 - \frac{1}{2\tau} \right) \left[\frac{\mathbf{e}_\alpha \cdot \mathbf{F}_m}{c_s^2} + \frac{\mathbf{e}_\alpha \cdot \mathbf{u}}{c_s^4} (\mathbf{e}_\alpha \cdot \mathbf{F}_m) - \frac{\mathbf{u} \cdot \mathbf{F}_m}{c_s^2} \right], \quad (2.6)$$

where ω_α is the weight parameter, defined as $\omega_0 = 4/9$, $\omega_{1-4} = 1/9$, $\omega_{5-8} = 1/36$, c_s is the lattice sound speed, and \mathbf{u} is the intrinsic phase-average velocity of fluid phase $\langle \mathbf{u}_f \rangle^f$. The macroscopic density ρ_f and velocity \mathbf{u} are calculated using

$$\rho_f = \sum_{\alpha=0}^8 f_\alpha \quad \text{and} \quad \rho_f \mathbf{u} = \sum_{\alpha=0}^8 \mathbf{e}_\alpha f_\alpha + \frac{1}{2} \delta t \rho_f \mathbf{F}_m. \quad (2.7a,b)$$

The macroscopic velocity equation in (2.7) is nonlinear in the velocity \mathbf{u} , since the total body force term \mathbf{F}_m includes \mathbf{u} . The quadratic equation is solved by introducing (2.2) into (2.7), and then the velocity \mathbf{u} is computed using

$$\mathbf{u} = \frac{\mathbf{v}}{d_0 + \sqrt{d_0^2 + d_1 |\mathbf{v}|}} + \mathbf{V}_p \quad \text{and} \quad \rho_f \mathbf{v} = \sum_{\alpha=0}^8 \mathbf{e}_\alpha f_\alpha + \frac{1}{2} \delta t \rho_f \mathbf{G} - \rho_f \mathbf{V}_p, \quad (2.8a,b)$$

where \mathbf{v} stands for the temporal variable and the two parameters d_0 and d_1 are $d_0 = (1 + (1/2)\delta t(\varepsilon\nu/K))/2$ and $d_1 = \delta t(\varepsilon^2 F_\varepsilon / \sqrt{K})/2$.

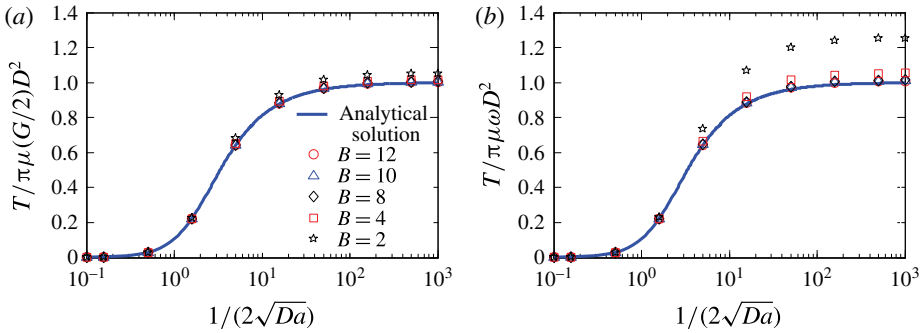


FIGURE 1. Dimensionless torque acting on a circular porous particle as a function of $1/(2\sqrt{Da})$ for various confinement ratios B at $Re_p = 0.08$: (a) the particle is stationary in simple shear flow of shear rate G ; (b) the particle has no translational motion but rotates with an angular velocity $G/2$ in a quiescent fluid.

The periodic boundary conditions are implemented in the flow direction (length direction), and the Zou–He boundary condition based on the bounceback of the non-equilibrium part of the distribution function (Zou & He 1997) is applied for the bounding walls (width direction). No explicit boundary condition is used for the interface between the porous particle regime and free flow, since a second-order viscous term is already included in the macroscopic governing equations. The fluid density ρ_f and particle density ρ_p are set to $\rho_f = \rho_p = 1.0$. We use both the stress integration method (Li *et al.* 2004) and the momentum exchange method (Mei, Yu & Shyy 2002) to compute the hydrodynamic drag force F_p^{drag} acting on the particle. After F_p and T_p are obtained, the translational and angular velocity, as well as the position, can be updated via (2.3). We find that the angular velocities at steady state based on two force evaluation methods, in the current work, are almost the same. The grid independence is also checked by the simulations of particle rotation in shear flow with $Re_p = 39.168$ and $Da = 4.25 \times 10^{-12}$, in which we consider relaxation times $\tau = 0.58, 0.60, 0.65, 0.70$, particle diameters $D = 40, 50, 60$ lattice size, and aspect ratios $W/H = 4, 6, 8$. The computed angular velocities at steady state for all the cases are very close to $0.3807(\pm\%0.03)$, and thus $W/H = 6, \tau = 0.58$ and $D = 50$ lattice size are chosen in the rest of this work.

3. Results and discussion

To validate our model, we first examine the torque acting on the porous particle at a near-zero particle shear Reynolds number ($Re_p = 0.08$) in two scenarios: (i) the particle is stationary in shear flow of shear rate G , and (ii) the particle has no translational motion but rotates with an angular velocity $\omega = G/2$ in a quiescent fluid. For such a small Re_p , the effect of fluid inertia is negligible. Various confinement ratios B ($= H/D, 2 \sim 12$) and Da ($2.5 \times 10^{-7} \sim 25$) are considered. The results are compared to the analytical solutions by Masoud *et al.* (2013), which are given by $T = -\pi\mu\omega D^2(I_2(1/\sqrt{4Da})/I_0(1/\sqrt{4Da}))$. Note that T is the magnitude of the torque, μ is the dynamic viscosity, and I_2 and I_0 are modified Bessel functions of the first kind. Figure 1 shows that the curves of dimensionless torque on the porous particle for $B = 10$ and 12 practically overlap, which means that the confinement effect due to the bounding walls can be neglected when $B \geq 10$. We also notice that the dimensionless torque for $B \geq 10$ agrees very well with the analytical solutions

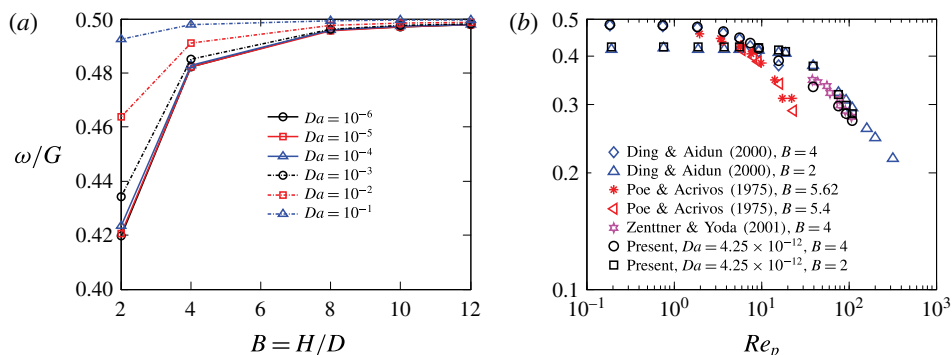


FIGURE 2. Dimensionless angular velocity ω/G (a) as a function of the confinement ratio B for various Da at $Re_p = 0.08$, and (b) as a function of Re_p for various B at $Da = 4.25 \times 10^{-12}$, compared with results for a solid impermeable particle in the literature.

by Masoud *et al.* (2013), thus confirming the accuracy of our model. By comparing figures 1(a) to 1(b), we find that the torque experienced by the particle rotating with an angular velocity of $G/2$ in scenario (ii) matches very well with the torque exerted by shear flow with shear rate of G on a stationary particle in scenario (i) in the absence of a confinement effect (i.e. $B \geq 10$). However, with an enhanced confinement effect (i.e. B decreasing from 10 to 2), the torque on the particle rotating in a quiescent fluid departs gradually from that for a stationary particle in shear flow with a shear rate of G . This suggests that the confinement ratio has an impact on the particle dynamics.

Then we study a porous particle freely rotating in shear flow between two bounding walls (with confinement ratio $B = 2 \sim 12$) at near-zero particle shear Reynolds number $Re_p = 0.08$. Here $Da = 10^{-6} \sim 10^{-1}$. Figure 2(a) shows the effect of B on the dimensionless angular velocity ω/G (normalized by the shear rate G). It is noted that ω/G increases with B , and converges to approximately 0.5 when $B \geq 10$, regardless of Da . For large $B (\geq 10)$, whereas the confinement effect is minute, we obtain $\omega/G = 0.49710 \sim 0.4996$ for $B = 10$ and $0.4978 \sim 0.4997$ for $B = 12$ when Da varies from 10^{-6} to 10^{-1} , which is in good agreement with the results for a solid impermeable particle in simple shear flow, i.e., the exact analytical solutions ($\omega/G = 0.5$ in unbounded domain by Jeffery (1922)) and numerical results ($\omega/G = 0.4982$ by Ding & Aidun (2000) and $\omega/G = 0.4971$ by Ku & Lin (2009) for $Re_p = 0.08$ and $B = 10$). This supports the conclusion by Masoud *et al.* (2013) that the permeability has little effect on the rotational behaviour of a porous particle at negligible particle shear Reynolds number in unbounded shear flow, where the Jeffery's prediction (Jeffery 1922) remains an excellent approximation for the angular velocity of porous particles. For smaller $B (< 10)$, where the confinement effect of the two bounding walls plays a role, we identify that ω/G is suppressed to below 0.5. Ding & Aidun (2000) found that for low Re_p the angular velocity of an impermeable solid particle in shear flow decreases when the width of the channel decreases. As shown in figure 2(a), we can draw a similar conclusion for a porous particle. However, the suppressing effect for the rotation of a porous particle is also dependent on Da when Re_p is low. The smaller Da , the lower ω/G . At $B = 2$, for instance, we find that ω/G for $Da = 10^{-6}$ is 15% lower than that for $Da = 10^{-1}$. This indicates that the effect of permeability on the rotation of a porous particle should not be neglected when the confinement ratio is small, even if the fluid inertia can be neglected.

Rotation of porous particle in shear flow with inertia

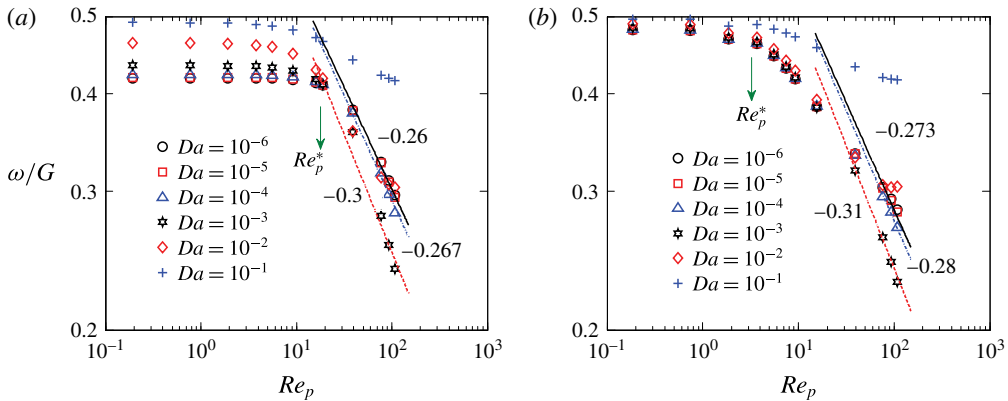


FIGURE 3. Comparison of the simulation results on the angular rate of a circular porous particle in a simple shear flow with various Darcy numbers at the same confinement ratio, (a) $B = 2$, (b) $B = 4$. Lines of slope -0.26 , -0.267 and -0.3 at $B = 2$, and slope -0.273 , -0.31 and -0.28 at $B = 4$ are also shown.

Next we investigate the effect of fluid inertia on the rotation of a porous particle in shear flow with Re_p up to 108. Here we limit B to 2 and 4 to illustrate the influence of confinement. First Da is fixed at $Da = 4.25 \times 10^{-12}$. Thus, the porous particle approximates its solid impermeable counterpart, and a comparison with results available in the literature for a solid impermeable particle can be made. As depicted in figure 2(b), we observe that the angular velocity of the particle decreases with increasing Re_p , as reported in many previous works (Kossack & Acrivos 1974; Poe & Acrivos 1975; Ding & Aidun 2000; Zettner & Yoda 2001). Quantitatively, our results for the angular velocity ω/G are in good agreement with the simulation results by Ding & Aidun (2000) for the whole range of Re_p studied in this work, which further demonstrates the accuracy of the current model. In particular, for low Re_p we find that ω/G reaches a plateau of 0.48 for $B = 4$ and 0.42 for $B = 2$, and the width of plateau varies with the confinement ratio B , which is $Re_p = 0 \sim 3$ for $B = 4$ and $Re_p = 0 \sim 20$ for $B = 2$. This was also well documented by Ding & Aidun (2000). For high $Re_p > 39$ we notice that the simulation results in this work agree well with the experimental results by Zettner & Yoda (2001) and numerical results by Ding & Aidun (2000), where ω/G decays rapid with Re_p .

We extend the range of Da to $10^{-6} \sim 10^{-1}$, and further examine the effects of fluid inertia and confinement on the rotation of a porous particle in shear flow. As shown in figure 3, the trend of ω/G decaying with increasing Re_p , similar to that for a solid impermeable particle, as shown in figure 2(b), is observed for both $B = 2$ and $B = 4$. A plateau of ω/G is also identified in figure 3 for various Da at low Re_p . Therefore, we argue that a critical Re_p , hereafter referred to as Re_p^* , can be defined to illustrate the importance of the effect of fluid inertia. In the case of $Re_p < Re_p^*$, ω/G remains almost constant with increasing Re_p , indicating that the Reynolds number has little effect on the rotation of the particle. For Re_p larger than Re_p^* , ω/G is significantly influenced by the Reynolds number, and decays rapidly with Re_p . From figure 3, we find that Re_p^* is 3 for $B = 4$ and 20 for $B = 2$, and Re_p^* is reduced when B increases, which suggests that the effect of Reynolds number on particle rotation must be considered even for very small Re_p in a wider channel. In fact, Kossack & Acrivos (1974) found that fluid inertia already plays a significant role for a solid impermeable particle in

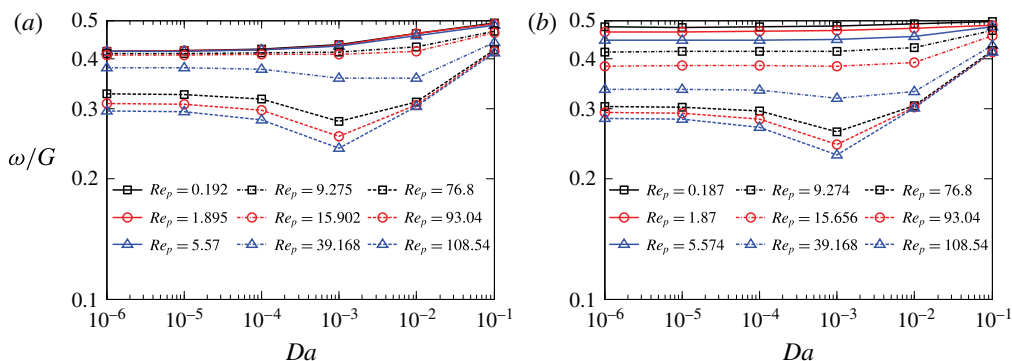


FIGURE 4. Dimensionless rotational angular velocity as a function of Da at various Re_p at the same confinement ratio (a) $B=2$, (b) $B=4$.

an unbounded shear flow with $Re_p = 1$. Comparison between figures 3(a) and 3(b) also shows that the confinement of two bounding walls suppresses ω/G to below 0.5. The smaller the confinement ratio B , the lower the angular velocity ω/G . This observation is in accordance with our results for $Da = 4.25 \times 10^{-12}$, as discussed above, and the results by Ding & Aidun (2000) and Zettner & Yoda (2001) for a solid impermeable particle. To summarize, the fluid inertia and the confined walls have similar effects on the rotation of a circular porous particle in shear flow as on a solid impermeable particle. In addition, we found there is a power law between ω/G and Re_p at smaller Da ($10^{-6} \leq Da \leq 10^{-3}$) when Re_p is larger than Re_p^* , but the power law is absent for $Da = 10^{-2}$ and 10^{-1} (as shown in figure 3). The power reduces (for example, from -0.26 to -0.3 for $B=2$) when Da increases from 10^{-6} to 10^{-3} , indicating a more rapid decay of ω/G with Re_p . The trend could be extrapolated to larger Re_p , but the results should be verified by further numerical work or experiments.

We also evaluate the effect of permeability on the rotation of a porous particle in shear flow at finite Re_p . For low $Re_p (< 20)$, as shown in figure 4, the angular velocity ω/G increases with Da . It is also seen that ω/G demonstrates the largest deviation from 0.5 (the theoretical value of ω/G for an impermeable particle rotating in an unbounded shear flow at $Re_p = 0$ by Jeffery (1922)) when $Da = 10^{-6}$, and the deviation is reduced with increasing Da . Thus, the suppression of the angular velocity ω/G due to the confinement of bounding walls is enhanced by reducing the permeability of the particle. We observe that the rate of increase of ω/G with Da at $B=2$ is higher than that at $B=4$. Masoud *et al.* (2013) found that Da has a negligible effect on ω/G in shear flow with a vanishing confinement effect and fluid inertia. Based on our results, together with the findings of Masoud *et al.* (2013), we expect that the increasing rate of ω/G with Da at low $Re_p (< 20)$ may reduce to a negligible amount when the confinement effect vanishes. Therefore, for low $Re_p (< 20)$, we argue that the rotation of the porous particle increases with Da in a bounded shear flow, and the rate of increase of angular velocity with Da diminishes when the confinement effect reduces. In the limit of unbounded flow, the increasing rate of angular velocity over Da becomes negligible, and Da has little effect on the rotation of a porous particle. For large $Re_p (> 20)$, ω/G is influenced by Da in a more complicated way, as shown in figure 4. With increasing Da , ω/G first drops slowly to a minimum, then rises rapidly. We observe the minimum of ω/G occurs at $Da = 10^{-3}$ for both $B=2$ and $B=4$ in our simulations.

Rotation of porous particle in shear flow with inertia

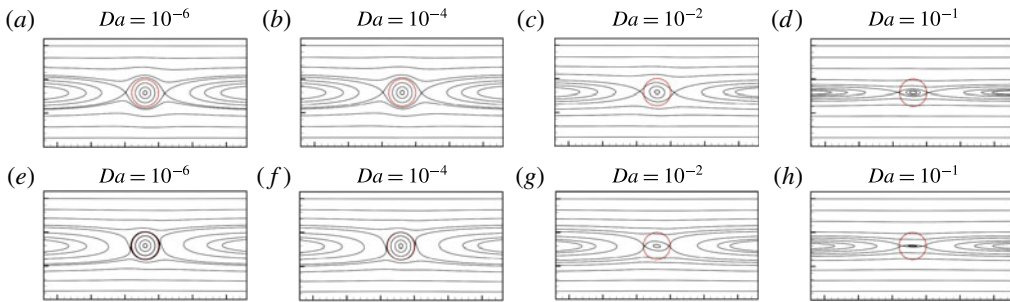


FIGURE 5. Streamlines for shear flow past a freely rotating circular porous particle with various Da and Re_p at $B = 4$, (a–d) for $Re_p = 5.574$, (e–h) for $Re_p = 76.8$. $B = 2$ presents similar results (not shown here).

To understand better the flow field inside and around the rotating porous particle, we plot typical results of the streamlines for the shear flow in figure 5. The streamlines for $B = 2$ and $B = 4$ are quite similar, so we show only the results for $B = 4$ in figure 5. We find that a particle with higher Da is effectively more permeable, indicating that the permeability has a strong influence on the flow field interior and exterior to the rotating particle in the shear flow at finite Re_p , as in the results without inertia given by Masoud *et al.* (2013). In addition, the flow pattern in figure 5 is similar to that of a solid particle freely rotating in shear flow given by Ding & Aidun (2000) and Zettner & Yoda (2001). For a solid impermeable particle, it is argued that the particle rotation is determined by a positive torque exerted by fluid flows adjacent to the two bounding walls moving in opposite directions, and a negative torque due to the recirculation of fluid flow in the middle of the channel (Ding & Aidun 2000; Zettner & Yoda 2001). Besides these two contributions, a third fluid layer moving near and around the particle at the surface exists, and transfers momentum from the moving walls and the recirculating flow to the particle, but the net effect of the fluid layer around the particle plays a minor role in reducing the particle rotation. For a porous particle, however, the flow that penetrates the particle plays an important role in the particle behaviour, i.e., many streamlines (which are dependent upon the permeability) can penetrate and pass through the particle, reducing the contribution to the angular velocity of the particle from the recirculation region. Thus, we examine the effect of fluid inertia and permeability on the flow rate through the particle. Since the flow rate through the entire particle is zero, based on the symmetrical flow field, we calculate the flow rate passing the top-half of the porous particle at steady state $Q_{porous} = U_{aver}D/2$ for all the cases, where U_{aver} stands for the average velocity along the top radius in the y -direction of the particle. To compare with the flow rates with various Re_p and Da , Q_{porous} is normalized by the flow rate through the top-half of an infinitely permeable particle (the porosity $\varepsilon = 1$), Q_{ip} . In figure 6, we find that the normalized flow rate decreases with increasing Re_p at the same Da with $B = 4$, and there also exists a critical Reynolds number Re_p^* . For $Re_p < Re_p^*$, the flow rate remains almost constant with increasing Re_p , and when $Re_p > Re_p^*$, the flow rate decays rapidly with Re_p . The reason may be that the normalized flow rate depends on the particle rotation at steady state, and the value of ω/G decreases with Re_p . We also find that the normalized flow rate increases with Da at various Re_p , indicating that the permeability strongly affects the flow rate through the particle. Additionally, the curves of normalized flow rates for $B = 2$ with various Re_p and Da present a similar trend.

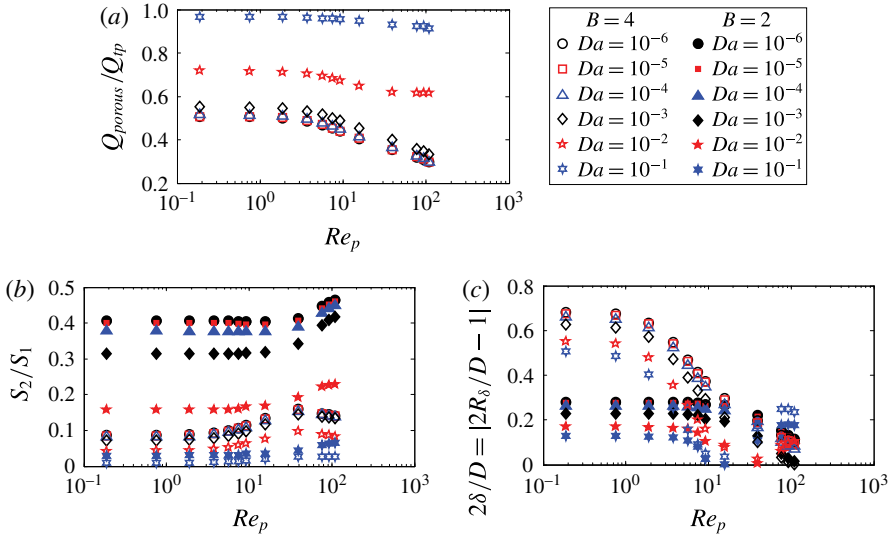


FIGURE 6. (a) Dimensionless flow rate at steady state Q_{porous}/Q_{tp} through the top-half of a porous particle as a function of Re_p at various Da with $B=4$; (b) value of S_2/S_1 as a function of Re_p at various Da and B ; (c) locations of the stagnation points as a function of Re_p at various Da and B , R_δ is the distance between the stagnation point and the centre of the particle.

Figure 5 shows that the location of the stagnation point and the area of recirculating flow change with Re_p , Da and B . Following Zettner & Yoda (2001), therefore, we present a simple scaling argument based on the balance of torque exerted by the fluid flow to explain the effects of B , Re_p and Da on ω/G . Similarly, one circular porous particle of diameter D rotating steadily at angular velocity ω in a channel of height H and the maximum shear velocity U on the wall is considered. We assume that the velocity profiles near the particle surface are roughly linear; thus, the positive torque contributed by the movement of the bounding walls is $T^+ \sim \mu(\Delta u_r/\Delta r)\Delta S \sim \mu((U - 0.5\omega D)/0.5(H - D))S_1 \sim \mu((B - \omega/G)/(B - 1)/G)S_1$, and the negative torque due to recirculation of fluid flow is $T^- \sim \mu(\Delta u_r/\Delta r)\Delta S \sim \mu(0.5\omega D/\delta)S_2 \sim \mu(\omega/G/(2\delta/(GD)))S_2$, where δ is the distance between the stagnation point and the centre of the particle surface, i.e., $\delta = |R_\delta - D/2|$, and R_δ is the distance between the stagnation point and the centre of the particle. S_1 and S_2 are the effective areas of the flow imposing the positive and negative torques on the particle, respectively. Noting that the steady ω/G in shear flow is actually a balance of the aforementioned positive and negative torque, we can estimate the angular velocity of the porous particle from the following simple scaling argument:

$$\omega/G \sim \frac{1}{0.5 \frac{S_2 D}{S_1 \delta} + \left(1 - 0.5 \frac{S_2 D}{S_1 \delta}\right) \frac{1}{B}} \sim \frac{B}{0.5 \frac{S_2 D}{S_1 \delta} (B - 1) + 1} \quad (3.1)$$

The values of S_2/S_1 and the dimensionless distance between the stagnation point and the particle surface are shown in figures 6(b) and 6(c), respectively, as a function of Re_p for various Da and B . In figure 6(b,c), we find that the value of S_2/S_1 is reduced as B increases, and thus the stagnation point moves gradually away from the

particle surface, resulting in an increase of ω/G based on (3.1). When B is larger than 10, the confinement effect can be omitted in (3.1). This explains the effect of the confinement ratio on the particle rotation. The explanation of the effect of Re_p is not as straightforward. However, Poe & Acrivos (1975) and Zettner & Yoda (2001) found that the influence of Re_p can be related to δ , the distance between the stagnation point and the particle external surface. For a particle with very small Da , i.e. fluid flow is hard to penetrate or pass through the particle, the ratio S_2/S_1 increases and the stagnation points of the recirculation flow become closer to the particle surface when Re_p increases (figure 6*b,c*), which in turn leads to a reduction of ω/G based on (3.1), resembling that for a solid impermeable particle (Ding & Aidun 2000; Zettner & Yoda 2001). This can be evidenced by comparing the streamlines in figures 5(*a*) and 5(*e*) or figures 5(*b*) and 5(*f*). For large Da , even though more fluid can penetrate the particle due to the effect of permeability (figures 6*d* and 6*h*), the value of S_2/S_1 also increases with Re_p . The combined effects of δ and S_2/S_1 with increasing Re_p eventually lead to a slow decrease of ω/G for a highly permeable particle ($Da = 10^{-1}$), as demonstrated in figure 3. The effect of Da can also be explained. Figure 4 depicts that ω/G increases with Da for low Re_p . As seen in figure 5(*a-d*), for $Re_p = 5.574$, the stagnation points stay outside of the particle, but when Da rises from 10^{-6} to 10^{-1} , more and more streamlines penetrate or pass through the particle. Thus, S_2/S_1 decreases as the recirculation area is gradually reduced, and we can expect a higher ω/G at steady state following (3.1). At high Re_p , with increasing Da , the stagnation points can move from outside to inside the particle, crossing the external surface of the particle, as shown in figure 5(*e-h*). In figure 6(*c*), we find that δ first drops and then increases after the stagnation points crossing the external surface of particle at high Re_p . This explains the existence of a minimum of ω/G when Da changes from 10^{-6} to 10^{-1} . For high Da , the reduction of the recirculation area results in a rapid increase of ω/G , as shown in figure 4.

4. Conclusions

We investigate the rotation of a circular porous particle in a shear flow with Re_p up to 108 by numerical simulations. The volume-averaged macroscopic momentum equation is used to formulate the fluid flow of a moving porous particle, and a modified single relaxation time lattice Boltzmann method is implemented to solve the macroscopic equation. The code is validated with the analytic solutions given by Masoud *et al.* (2013) for the rotation of a porous particle in unbounded shear flow at near-zero Re_p , and simulation and experimental data given by Ding & Aidun (2000), Zettner & Yoda (2001) for a solid impermeable particle with Re_p up to 108. The effects of fluid inertia, confinement ratio, and permeability are studied. Our results confirm the conclusion by Masoud *et al.* (2013) that the permeability has little effect on the rotation of a porous particle in unbounded shear flow without fluid inertia, but also suggest that the role of permeability cannot be neglected when the confinement effect is significant, or the fluid inertia cannot be neglected. The fluid inertia and the confining walls have similar effects on the rotation of a porous particle as they have on a solid impermeable particle. The angular velocity ω/G decays with increasing Re_p , and the confinement effect suppresses ω/G to below 0.5. The smaller the confinement ratio B , the lower the ω/G . The effect of fluid inertia on the rotation of particle is significant for $Re_p > Re_p^*$, where the critical Re_p^* decreases with the width of channel, and becomes minute when $Re_p \leq Re_p^*$. The permeability impacts the rotation of a porous particle in a more complicated way in bounded flow.

For low Re_p , ω/G increases with Da . For large Re_p , ω/G as function of Da first drops slowly to a minimum, then rises rapidly. Following Zettner & Yoda (2001), we find that a simple scaling argument based on the balance of a positive torque exerted by fluid flows adjacent to the two bounding walls and a negative torque due to the recirculation of fluid flow in the middle of the channel can explain our results.

Acknowledgement

This work is funded by the National Natural Science Foundation of China (grant no. 91334205).

References

- BHATTACHARYYA, B., DHINAKARAN, S. & KHALILI, A. 2006 Fluid motion around and through a porous cylinder. *Chem. Engng Sci.* **61**, 4451–4461.
- BLUEMINK, J. J., LOHSE, D., PROSPERETTI, A. & VAN WIJNGAARDEN, L. 2008 A sphere in a uniformly rotating or shearing flow. *J. Fluid Mech.* **600**, 201–233.
- BRINKMAN, H. C. 1949 A calculation of the viscous force exerted by a flowing fluid on a dense swarm of particles. *Appl. Sci. Res.* **1**, 27–34.
- BYRON, M., EINARSSON, J., GUSTAVSSON, K., VOTH, G., MEHLIG, B. & VARIANO, E. 2015 Shape-dependence of particle rotation in isotropic turbulence. *Phys. Fluids* **27**, 035101.
- CHEN, C. B. & CAI, A. 1999 Hydrodynamic interactions and mean settling velocity of porous particles in a dilute suspension. *J. Colloid Interface Sci.* **217**, 328–340.
- CHEN, S. & DOOLEN, G. D. 1998 Lattice Boltzmann method for fluid flows. *Annu. Rev. Fluid Mech.* **30**, 329–364.
- DALWADI, M. P., CHAPMAN, S. J., WATERS, S. L. & OLIVER, J. M. 2016 On the boundary layer structure near a highly permeable porous interface. *J. Fluid Mech.* **798**, 88–139.
- DEBYE, P. & BUECHE, M. 1948 Intrinsic viscosity, diffusion, and sedimentation rate of polymers in solution. *J. Chem. Phys.* **16**, 573–579.
- DING, E. J. & AIDUN, C. K. 2000 The dynamics and scaling law for particles suspended in shear flow with inertia. *J. Fluid Mech.* **423**, 317–344.
- ERGUN, S. 1952 Fluid flow through packed columns. *Chem. Engng Prog.* **48**, 89–94.
- JEFFERY, G. B. 1922 The motion of ellipsoidal particles immersed in a viscous fluid. *Proc. R. Soc. Lond. A* **102**, 161–179.
- KLEIN, S., GIBERT, M., BÉRUT, A. & BODENSCHATZ, E. 2013 Simultaneous 3d measurement of the translation and rotation of finite-size particles and the flow field in a fully developed turbulent water flow. *Meas. Sci. Technol.* **24**, 1–10.
- KOSSACK, C. A. & ACRIVOS, A. 1974 Steady simple shear flow past a circular cylinder at moderate Reynolds numbers: a numerical solution. *J. Fluid Mech.* **66**, 353–376.
- KU, X. K. & LIN, J. Z. 2009 Inertial effects on the rotational motion of a fibre in simple shear flow between two bounding walls. *Phys. Scr.* **80**, 025801.
- LADD, A. J. C. 1994 Numerical simulations of particulate suspensions via a discretized Boltzmann equation. part 2. numerical results. *J. Fluid Mech.* **271**, 311–339.
- LI, H., LU, X., FANG, H. & QIAN, Y. 2004 Force evaluations in lattice Boltzmann simulations with moving boundaries in two dimensions. *Phys. Rev. E* **70**, 026701.
- LIN, C. J., PEERY, J. H. & SCHOWALTER, W. R. 1970 Simple shear flow round a rigid sphere: inertial effects and suspension rheology. *J. Fluid Mech.* **44**, 1–17.
- MAO, W. B. & ALEXEEV, A. 2014 Motion of spheroid particles in shear flow with inertia. *J. Fluid Mech.* **749**, 145–166.
- MASOUD, H., STONE, H. A. & SHELLEY, M. J. 2013 On the rotation of porous ellipsoids in simple shear flows. *J. Fluid Mech.* **733**, R6.
- MATHAI, V., NEUT, M. W. M., VAN DER POEL, E. P. & SUN, C. 2016 Translational and rotational dynamics of a large buoyant sphere in turbulence. *Exp. Fluids* **57**, 51.

Rotation of porous particle in shear flow with inertia

- MEI, R., YU, D. & SHYY, W. 2002 Force evaluation in the lattice Boltzmann method involving curved geometry. *Phys. Rev. E* **65**, 041203.
- MICHALOPOULOU, A. C., BURGANOS, V. N. & PAYATAKES, A. C. 1993 Hydrodynamic interactions of two permeable particles moving slowly along their centerline. *Chem. Engng Sci.* **48**, 2889–2900.
- NEALE, G. & EPSTEIN, N. 1973 Creeping flow relative to permeable spheres. *Chem. Engng Sci.* **28**, 1865–1874.
- OLLILA, S. T. T., ALA-NISSILA, T. & DENNISTON, C. 2012 Hydrodynamic forces on steady and oscillating porous particles. *J. Fluid Mech.* **709**, 123–148.
- POE, G. G. & ACRIVOS, A. 1975 Closed-streamline flows past rotating single cylinders and spheres: inertia effects. *J. Fluid Mech.* **72**, 605–623.
- ROBERTSON, C. R. & ACRIVOS, A. 1970 Low Reynolds number shear flow past a rotating circular cylinder. part I. momentum transfer. *J. Fluid Mech.* **40**, 685–703.
- ROY, B. C. & DAMIANO, R. 2008 On the motion of a porous sphere in a Stokes flow parallel to a planar confining boundary. *J. Fluid Mech.* **606**, 75–104.
- SHAHSVARI, S., WARDLE, B. & MCKINLEY, G. H. 2014 Interception efficiency in two-dimensional flow past confined porous cylinders. *Chem. Engng Sci.* **116**, 752–762.
- WANG, L., WANG, L. P., GUO, Z. & MI, J. 2015 Volume-averaged macroscopic equation for fluid flow in moving porous media. *Intl J. Heat Mass Transfer* **82**, 357–368.
- WOOD, B. D. 2007 Inertial effects in dispersion in porous media. *Water Resour. Res.* **43**, W12S16.
- WU, Y., WU, X., YAO, L., BRUNEL, M., COETMELLEC, S., LEBRUN, D., GREHAN, G. & CEN, K. 2015 Simultaneous measurement of 3d velocity and 2d rotation of irregular particle with digital holographic particle tracking velocimetry. *Powder Tech.* **284**, 371–378.
- ZETTNER, C. M. & YODA, M. 2001 The circular cylinder in simple shear at moderate Reynolds numbers: An experimental study. *Exp. Fluids* **30**, 346–353.
- ZIMMERMANN, R., GASTEUIL, Y., BOURGOIN, M., VOLK, R., PUMIR, A. & PINTON, J. 2011 Rotational intermittency and turbulence induced lift experienced by large particles in a turbulent flow. *Phys. Rev. Lett.* **106**, 154501.
- ZOU, Q. & HE, X. 1997 On pressure and velocity boundary conditions for the lattice Boltzmann BGK model. *Phys. Fluids* **9**, 1591–1598.